INTERNATIONAL JOURNAL OF PRECISION ENGINEERING AND MANUFACTURING Vol. 17, No. 3, pp. 347-353 MARCH 2016 / 347
DOI: 10.1007/s12541-016-0043-7 ISSN 2234-7593 (Print) / ISSN 2005-4602 (Online)

Development of Magnetic/Non-Magnetic Stainless Steel Parts Produced by Two-Component Metal Injection Molding

Marco Mulser[1,#], Georg Veltl[1], and Frank Petzoldt[1]

1 Fraunhofer Institute for Manufacturing Technology and Advanced Materials - IFAM, Wiener Str. 12, 28359 Bremen, Germany
Corresponding Author / E-mail: marco.mulser@ifam.fraunhofer.de, TEL: +49-421-2246-231, FAX: +49-421-2246-300

KEYWORDS: Co-sintering, Interdiffusion, Magnetic/non-magnetic, Sinterdilatometry, Two-component metal injection molding

The paper describes results that were achieved by joining the ferritic stainless steel AISI 430 and the austenitic stainless steel AISI 314 by two-component metal injection molding. Sinterdilatometry was used to compare the sintering response of the materials. To compensate discrepancies in shrinkage during co-sintering, several gas-atomized powder fractions were combined. Using this approach, feedstock combinations which did not exceed a shrinkage mismatch of 5% were processed into micro tensile test specimens by sequential or simultaneous co-injection molding. The ferritic/austenitic interfaces were characterized with a focus on interdiffusion of alloying elements and mechanical properties. Defect-free and well-connected bi-material specimens with magnetic/non-magnetic properties were obtained. Results showed that the interdiffusion between the utilized steels resulted in a local strengthening effect that increased the hardness and mechanical properties of the interface. The tensile strength was comparable to the strength of the base material and all specimens failed outside the interface. It demonstrates that the investigated material combination is suitable to produce magnetic/non-magnetic parts by two-component metal injection molding.

Manuscript received: June 12, 2015 / Revised: October 28, 2015 / Accepted: November 24, 2015

1. Introduction

Metal Injection Molding (MIM) is an established manufacturing technology for net-shape components with tight tolerances. In general, it is applied to produce complex-shaped metal parts of high-precision and is especially efficient in high volume production.[1] The majority of MIM components are made of iron-based materials such as low-alloy steels, stainless steels or tool steels but also non-ferrous metals as titanium, copper and tungsten alloys or cemented carbides are processed with increasing demand.[2,3] After manufacturing, MIM components are usually mounted to other components to fulfil multiple functions as part of an assembly. Nevertheless, most MIM parts are still restricted to monolithic materials.

About two decades ago, investigations were initiated to establish the two-component metal injection molding (2C-MIM) that was adapted from plastic injection molding.[4-6] The technology allows manufacturing bi-material MIM components with tailored properties.[7] Additional joining or coating steps that are usually involved in conventional MIM can be eliminated so that functionally graded components can be manufactured at attractive costs. It provides new design opportunities and advanced functionality options for engineers and designers of technical products. Thus, unique properties can be combined in a single component such as high toughness and wear resistance,[8-10] magnetic and non-magnetic properties,[11] local hollow structures in dense components[12] or flexible, non-detachable connections.[13] In general, a twin-barrel injection molding machine is used for molding 2C-MIM parts. The feedstocks are injected through two independent injection units either sequentially by using a core that blocks a certain part of the cavity or by simultaneous co-injection. In both cases the feedstocks are joined during shaping whereas the final bonding is obtained during co-sintering.

Two powder materials are suitable for 2C-MIM and co-sintering if they form a metallurgical bond at the interface and the sintering response is compatible. The technical challenge is to develop powders and feedstocks that experience similar sintering shrinkage. It has already been demonstrated, that major discrepancies in shrinkage induce differential stresses and provoke defects such as cracks, delamination and distortion at the interface.[14,15] That means that no

Table 1 Chemical composition in wt-% of AISI 430 and AISI 314

	Cr	Ni	Si	Mn	C	P	S	Fe
AISI 430	16.1	-	0.96	0.57	0.015	0.015	0.005	Bal.
AISI 314	22.0	22.0	2.00	1.30	0.150	0.017	0.006	Bal.

Table 2 Particle size of the utilized stainless steel powders

Powder		Particle size d_{90} [μm]
AISI 430	<7 μm	7.0
	<16 μm	15.8
	<32 μm	28.3
	<45 μm	48.2
AISI 314	<7 μm	7.0
	<16 μm	16.0
	<32 μm	33.0
	<45 μm	48.7

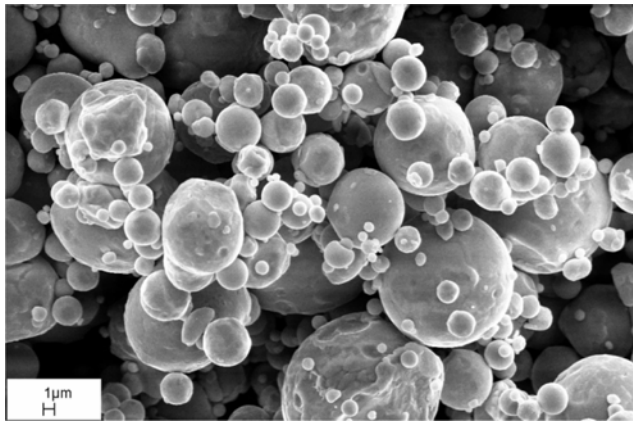

Fig. 1 SEM image of the stainless steel powder AISI 430 (<16 μm)

standard “ready-to-mold” feedstocks can be utilized. Instead customized feedstocks need to be developed that are compatible along the whole process chain including co-injection, co-debinding and co-sintering. Since the materials are processed in a single co-sintering cycle, a compromise concerning heating rate, sintering temperature, holding time and atmosphere is required.

Several investigations have shown that sinterdilatometry is a valuable tool to analyze and compare the sintering response.[16,17] To compensate the shrinkage of powders with different sintering characteristics several options can be applied. For instance the solids loading of feedstocks,[11] the utilized particle size,[10,18] additional alloying elements to stimulate the sintering behavior,[9,19] or modifications of the sintering cycle to minimize damage during heating,[9,18] can be utilized to balance the sintering response. So far, several material and property combinations have been studied for potential 2C-MIM applications including metals, ceramics and composites.[3,7,20] Investigations and case studies showed that 2C-MIM is a suitable process to combine two powder materials. However, only little data was published yet containing interface characterization and mechanical properties of the developed combinations.

In this study, the ferritic stainless steel AISI 430 (X6Cr17) and the austenitic steel AISI 314 (X16CrNi25-20) were investigated to produce magnetic/non-magnetic stainless steel parts by two-component MIM. Both materials are known to provide good corrosion resistance against corrosive environments such as salt spray and ethanol containing fuel due to their Cr content above 13%.[21]

2. Experimental Procedure

Pre-alloyed, gas-atomized powders with the chemical composition as listed in Table 1 were supplied by Sandvik Osprey Ltd., UK. Both powders were produced in several particle size distributions of <7 μm, <16 μm, <32 μm and <45 μm as shown in Table 2 together with the measured particle size by laser diffractometry. Fig. 1 shows exemplarily an SEM image of the spherical particles of the powders.

MIM feedstocks were prepared with a multi-component binder system that consists of a mixture of polyethylene (PE), waxes and stearic acid. Due to the spherical particle shape and high wax content, a high powder load of 69 vol.-% still provided sufficient feedstock flowability. The same binder composition was utilized for all powders and the powder load was kept constant for all feedstocks. Powders and binders were pre-mixed in a high speed laboratory mixer (Lödige TGHK 5, Germany) at 120°C for 30 min. The mixture was homogenized by applying high shear forces on a shear roll extruder and then granulated on the same equipment (Bellaform BSW 135-1000, Germany).

The sintering response of all feedstocks was examined by sinterdilatometry. For this, cylindrical dilatometry samples of 4 mm in diameter and 8 mm in height were molded on a vertical piston injection machine (HEK, Germany). The binders were removed by solvent extraction and thermal decomposition. The sintering shrinkage was monitored on a vertical pushrod dilatometer (Bähr TMA 801, Germany) in hydrogen atmosphere heating with 5 K min^{-1} to 1350°C and holding for 60 min. The cooling cycle with 10 K min^{-1} was monitored till 315°C.

To characterize the interface and to verify mechanical properties, micro tensile test specimens were molded with an interface area of 1.0×1.0 mm^2 in the green part. Injection molding was carried out on a twin-barrel injection molding machine equipped with a horizontal and a vertical injection unit and a screw diameter of 18 mm (Arburg Allrounder 320S 500-60, Germany). The process options sequentially injection molding and simultaneous co-injection were applied to produce specimens. For sequentially injection molding, half of the cavity was blocked by a core while the first feedstock was injected. After solidification, the core was retracted from the cavity and the second feedstock was injected to complete the specimen. Simultaneous co-injection was done without the core, so that the feedstocks were joined in the liquid state. To merge the feedstocks in the center of the specimen, the injections were adjusted to the velocity of the melt fronts by defining a delay time. Monolithic one-component specimens of both alloys were produced on the same equipment by utilizing just one of the injection units. For all experiments, the nozzle side was heated to higher temperatures than the ejector side to facilitate ejection of the specimens after molding. All relevant process parameters are listed in Table 3.

The tensile test specimens were debinded in a two-step debinding

Table 3 Injection molding parameters for sequentially injected, simultaneously co-injected and one-component specimens

	Sequentially injected and co-injected	One-component specimens
Feedstock temperature	100°C	92°C
Mold temperature (ejector / nozzle side)	37°C / 47°C	30°C / 40°C
Injection speed	60 mm s^{-1}	60 mm s^{-1}
Packing pressure	500 bar	650 bar

process. At first, the wax ingredients were extracted in hexane for four hours at RT. The mass loss was monitored to assure that at least 95% of the waxes were extracted. The PE backbone was removed by thermal decomposition in a batch furnace (MIM 3002, Elnik Systems, US) by applying a heating rate of 2 K min^{-1} and a holding time of 60 min at 700°C. After that, sintering was conducted with 600 mbar in hydrogen atmosphere with a heating rate of 5 K min^{-1} to 1340°C and a holding time of 120 minutes. The furnace was cooled to RT with 15 K min^{-1}.

The density was measured by fluid displacement (Archimedes' principle) in ethanol on a precision balance (Delta Range XS603S, Mettler Toledo, Switzerland). The microstructure was investigated using an optical light-microscope (Leica DMRX, Leica Microsystems, Germany). The surface of the sintered specimens was prepared by grinding on a gradual sequence of SiC emery papers and polishing with diamond paste. The specimens were etched at 50°C for less than 60 s in standard V2A etching solution. Scanning electron microscopy (SEM) in conjunction with energy-dispersive X-ray (EDX) analysis was performed across the interface of etched specimens. EDX point measurements of the elements Cr, Ni, Si and Mn were performed perpendicular to the interface every 5 μm along 600 μm.

Micro hardness was determined across the interface every 50 μm along 700 μm using Vickers hardness HV0.1 (LM 248 AT, Leco, US). The mechanical strength at room temperature was determined on an electromechanical tensile testing machine (Tensor, Innowep, Germany). At least five specimens of each type of two-component and one-component specimens were measured using a constant traverse speed of 2 mm min^{-1}. The elongation was determined by measuring the plastic deformation on tested specimens.

3. Results and Discussion

3.1 Sinterdilatometry

Fig. 2 shows the linear shrinkage against temperature of selected powder fractions. Table 4 summarizes characteristic values derived from the graphs including the temperature at 0.1% shrinkage $T_{(0.1\%)}$, the maximum shrinkage rate $\dot{s}_{max}$ and the temperature at maximum shrinkage rate $T_{(\dot{s}_{max})}$.

Indicated by $T_{(0.1\%)}$, it can be noticed that the AISI 430 requires lower temperatures to start sintering compared to AISI 314. Besides, the densification in AISI 430 is faster than in AISI 314 as can be recognized by $\dot{s}_{max}$. The results demonstrate also that the sintering response of both steels depends on the utilized particle size. The powders of finer particles start sintering at lower temperatures and

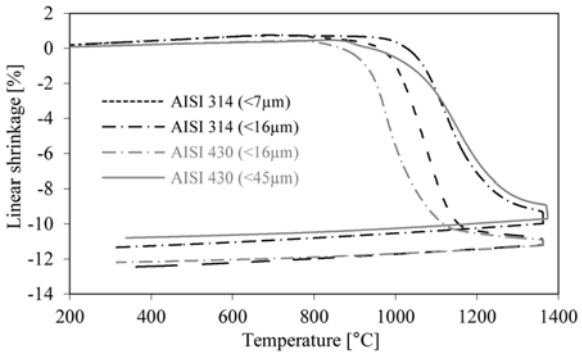

Fig. 2 Linear shrinkage against temperature

reveal a much faster densification with a higher maximum shrinkage rate compared to the utilized coarser particles. It is well known, that fine powders have a higher sinter activity due to their higher free surface energy than coarser particles.[22]

Other studies showed that a considerable mismatch in sintering response can induce undesirable strain during co-sintering. The strain induces biaxial stresses at the interface that causes distortion and cracks. Especially, a mismatch in the initial stage of sintering causes defects at the interface. Once the binder is removed and only powder particles remain, the strength of the MIM part reaches its minimum right before initial sintering begins.[9,15] Thus, besides a similar final shrinkage it is important that the shrinkage starts in the same temperature range.

By means of the sinterdilatometry values, feedstock combinations with similar shrinkage characteristics were selected. Combination C1 was defined as AISI 430 of the coarse powder fraction (<45 μm) combined with AISI 314 (<16 μm) and combination C2 was composed of AISI 430 (<16 μm) and the finest powder fraction of AISI 314 (<7 μm). The shrinkage mismatch during the heating cycle was determined graphically from Fig. 2. C1 reveals a maximum shrinkage mismatch of 0.91% at 1019°C and C2 a maximum shrinkage mismatch of 4.81% at 1016°C during heating.

3.2 Shrinkage and density

In Table 5 the final shrinkage and density values measured on one-component specimens are listed. As expected from dilatometry, the specimens of finer particle size in combination C2 show a higher shrinkage than the coarser powders of combination C1. Thus, in combination C2 the densification of both steels was higher than in combination C1. The densification of AISI 430 is only slightly higher than AISI 314 in both selected combinations.

3.3 Micrographs

Fig. 3 shows exemplarily a micrograph of the interface area of a sequentially injected micro tensile specimen of combination C2 after etching. The materials are well-connected and a crack-free interface was achieved. The uniform thickness of the specimen demonstrates that the shrinkage in thickness was balanced sufficiently. It confirms the predictions derived from dilatometry and shrinkage measurements. Even the shrinkage mismatch during heating did not harm the integrity of the interface. In the AISI 430 a diffusion layer with a lamellar

Table 4 Characteristic sintering parameters of the investigated powder fractions

Powder		$T_{(0.1\%)}$ [°C]	max [% min^{-1}]	$T_{(max)}$ [°C]
AISI 430	<7 μm	867	-0.63	984
	<16 μm	878	-0.42	973
	<32 μm	870	-0.25	976
	<45 μm	955	-0.22	1152
AISI 314	<7 μm	968	-0.38	1078
	<16 μm	1034	-0.29	1122
	<32 μm	1003	-0.14	1039
	<45 μm	1032	-0.14	1057

Table 5 Final shrinkage and density of one-component specimens after sintering at 1340°C for 120 min

	Specimens	Shrinkage [%]	Density [%]
C1	AISI 430 (<45 μm)	11.0	95.3
	AISI 314 (<16 μm)	11.0	96.0
C2	AISI 430 (<16 μm)	11.6	98.3
	AISI 314 (<7 μm)	11.9	97.9

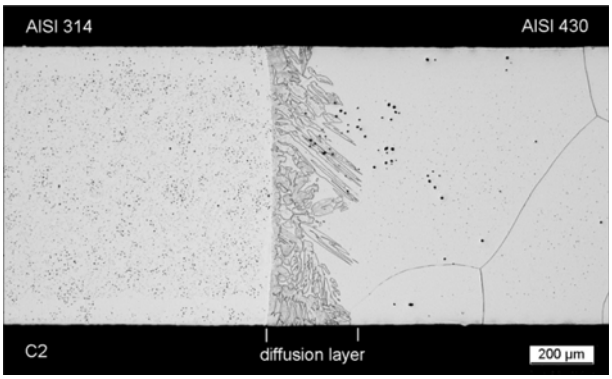

Fig. 3 Interface of a sequentially injected specimen

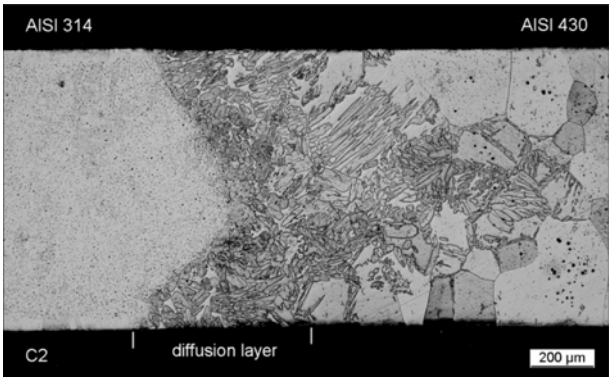

Fig. 4 Interface of a simultaneously co-injected specimen

structure can be identified that can be clearly distinguished from the microstructure of the base materials. The thickness of the diffusion layer is about 250 μm.

Also the simultaneously co-injected specimens of the same feedstock combination C2 revealed a sound interface without defects or major distortion (Fig. 4). In contrast to the straight and narrow interface of the sequentially injected specimen, it revealed a curved interface profile. The diffusion layer was much thicker. The AISI 314 penetrated the AISI 430 while both feedstocks were in the liquid state. It was already shown in other publications that the interface during co-injection is sensitive to the applied injection molding conditions.[6,23,24]

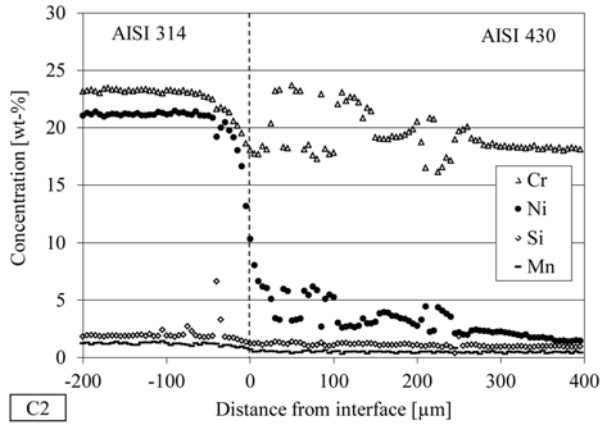

Fig. 5 Concentration of alloying elements across the interface measured by EDX on a sequentially injected specimen

3.4 Interdiffusion

Fig. 5 shows the Cr, Ni, Si and Mn concentration across the interface of a sequentially injected specimen of combination C2. Due to the fact that the austenitic steel AISI 314 is higher alloyed especially in Cr and Ni, the interdiffusion of the main alloying elements took place from AISI 314 to AISI 430. That is why, the AISI 314 was only influenced near the interface, whereas the interdiffusion into the AISI 430 shows a thickness of about 250 μm. In the diffusion layer the Cr and Ni concentration is not uniform. It is locally enriched with Cr up to 24 wt-% and Ni up to 7 wt-%. Where the Cr content is high, the Ni content is low and vice versa.

An approach to estimate the phase composition of interfaces between stainless steels is the Schaeffler diagram. Originally, it was established to estimate the weldability of steels with welding consumable after fast cooling directly after joining.[25-27] In this case, it can only provide a rough estimation of the phase composition for the bi-materials due to much slower cooling conditions after co-sintering.[16,28] In general, a Ni equivalent representing the austenite forming elements including Ni, C and Mn and a Cr equivalent representing the major ferrite formers including Cr, Mo, Si, Nb and Ti is calculated from chemical composition. In Fig. 6 the base materials AISI 430 and AISI 314 as well as the results of the EDX analysis were plotted in the Schaeffler diagram. The carbon content was assumed as in the base materials (see Table 1). The diagram reveals that the diffusion layer of the originally ferritic steel AISI 430 still consists of regions of ferrite. However, for the regions of high Ni and low Cr content a multi-phase austenitic, martensitic and ferritic microstructure is predicted. Obviously, the diffusion of Ni from AISI 314 into AISI 430 resulted in an increase of austenitic phase in the interface, whereas the diffusion of Cr into AISI 430 stabilized the ferrite phase. Due to the low carbon content and the low cooling rate of about 15 K min^{-1} it can be assumed that no martensite was formed and a dual-phase austenitic-ferritic microstructure was generated.[27] Due to

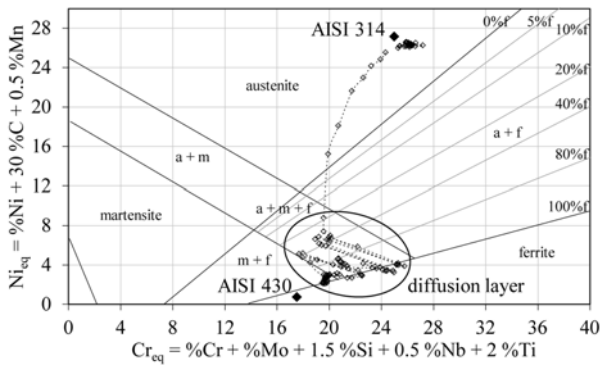

Fig. 6 Schaeffler diagram including the results of EDX analysis in the diffusion layer between AISI 314 and AISI 430

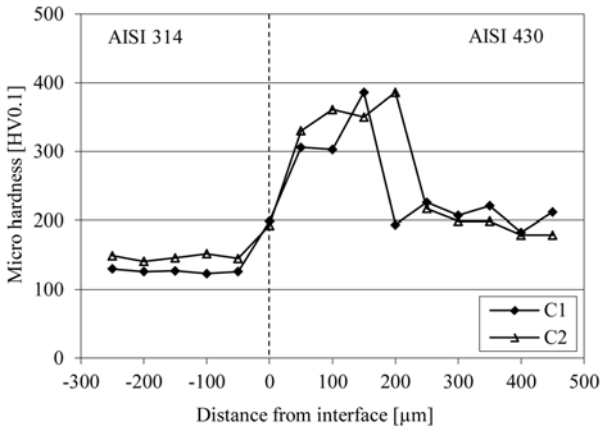

Fig. 7 Hardness profiles across the interface of sequentially injected specimens

continuous cooling with 15 K min^{-1} from sintering temperature to RT, it can also be assumed that no brittle sigma-phase was formed which is well known to be formed during welding processes between ferritic and austenitic steels and can deteriorate the mechanical properties of the joint. [26]

3.5 Mechanical properties

Fig. 7 shows the micro hardness profiles measured perpendicular to the interface of the sequentially injected specimens. C1 and C2 show a similar profile and indicate the effect of interdiffusion of alloying elements. The AISI 314 shows a constant hardness of about 140 HV0.1 that was not influenced by interdiffusion even close to the interface. It confirms the results of the EDX analysis that revealed only minor influence of interdiffusion on the AISI 314. However, the diffusion layer in AISI 430 reveals a significant increase in hardness from about 200 HV0.1 to more than 300 HV0.1. It is well known, that small additions of alloying elements influence the hardness of ferritic steels and especially Si, Mn and Ni increase the hardness of alpha iron significantly.[27] It can also be assumed, that the dual-phase austenitic-ferritic microstructure at the interface provides a strain hardening effect which results in an increase in hardness.

In Table 6 the mechanical properties of sequentially injected specimens are listed. The ultimate tensile strength (R_m) and the elongation at failure (A) of both combinations are shown in comparison to the properties of monolithic one-component specimens. It is important to mention that all tested specimens failed outside of the interface. In other words, all specimens failed in the ferritic stainless steel without any exception. Fig. 8 shows a typical two-component tensile specimen after injection molding, after co-sintering and after tensile testing. It visualizes that the interface was still intact after testing. Apparently, the interdiffusion of alloying elements and its influence on the microstructure caused not only an increase in hardness it also strengthened the interface. The results also confirm the assumption that no brittle sigma-phase was formed at the interface otherwise the interface had failed.

Table 6 Mechanical properties of sequentially injected specimens and one-component specimens (including standard deviation)

	Specimens	R_m [N mm^{-2}]	A [%]
C1	AISI 430 (<45 μm) + AISI 314 (<16 μm)	338 (7)	27.1 (1.7)
	AISI 430 (<45 μm)	342 (9)	20.2 (2.1)
	AISI 314 (<16 μm)	462 (3)	58.6 (1.2)
C2	AISI 430 (<16 μm) + AISI 314 (<7 μm)	342 (10)	26.0 (2.1)
	AISI 430 (<16 μm)	327 (14)	19.7 (2.6)
	AISI 314 (<7 μm)	522 (8)	61.8 (1.0)

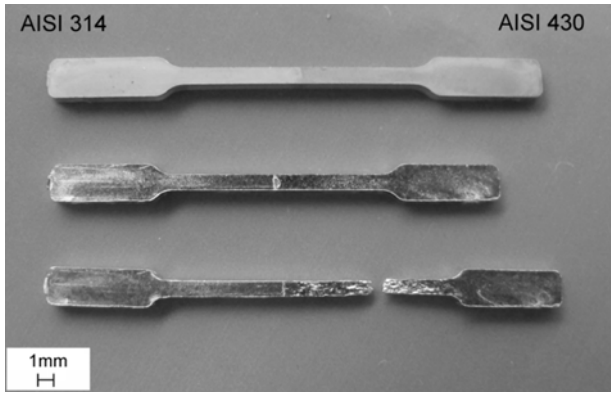

Fig. 8 Micro tensile specimens after injection molding, after co-sintering and after tensile testing

Both combinations show a tensile strength that is comparable to the strength of the one-component specimens of AISI 430 considering the standard deviation. Strength and elongation are in the same range as those in specifications but slightly lower than achieved by other authors.[29,30] It can be assumed that the properties can be improved by optimizing the sintering parameters and controlling the grain size of the AISI 430 since it is well known that long holding times result in grain growth and degrade the mechanical properties.[1]

4. Conclusions

The feasibility of two-component MIM for magnetic/non-magnetic bi-material parts was shown with a new stainless steel combination of

AISI 430 and AISI 314. From the results achieved the following conclusions can be drawn:

- Matching the particle size by using sinterdilatometry is an effective method to compensate the sintering response without modifying the chemical composition. This procedure allowed defining feedstock combinations of AISI 430 and AISI 314 with a shrinkage mismatch at less than 5% during heating.
- It was possible to produce well-connected and defect-free two-component specimens with a sound interface by sequentially injection and simultaneous co-injection molding.
- Due to interdiffusion of Ni and Cr a dual-phase lamellar microstructure was generated between the materials that had a strengthening effect on the interface. The microstructure of the diffusion layer increased the local hardness and mechanical strength so that the failure during tensile testing was always outside the interface.

ACKNOWLEDGEMENT

Parts of this study were funded by the German Federal Ministry of Education and Research (BMBF) within the Framework Concept ”Research for Tomorrow’s Production” (funding number 02PU2211) and managed by the Project Management Agency Karlsruhe (PTKA). The authors are responsible for the content of this publication.

REFERENCES

1. German, R. M. and Bose, A., “Injection Molding of Metals and Ceramics,” Metal Powder Industries Federation, pp. 12-13, 227-229, 1997.
2. Williams, B., “Powder Metallurgy - A Global Market Review,” International Powder Metallurgy Directory, 15th Ed., pp. 90-91, 2012.
3. Heaney, D. F., “Handbook of Metal Injection Molding,” Elsevier, pp. 32-34, 2012.
4. Pest, A., Petzoldt, F., Eifert, H., Veltl, G., Hartwig, T., and German, R. M., “Composite Parts by Powder Injection Molding,” Advances in Powder Metallurgy and Particulate Materials, Vol. 5, pp. 171-178, 1996.
5. Alcock, J., Logan, P., and Stephenson, D., “Metal Co-Injection Moulding,” Journal of Materials Science Letters, Vol. 15, No. 23, pp. 2033-2035, 1996.
6. Alcock, J., Logan, P., and Stephenson, D., “Surface Engineering by Co-Injection Moulding,” Surface and Coatings Technology, Vol. 105, No. 1, pp. 65-71, 1998.
7. Petzoldt, F., “Multifunctional Parts by Two-Component Powder Injection Moulding (2C-PIM),” Powder Injection Moulding International, Vol. 4, No. 1, pp. 21-27, 2010.
8. Johnson, J. L., Tan, L. K., Suri, P., and German, R. M., “Design Guidelines for Processing Bi-Material Components via Powder-Injection Molding,” JOM, Vol. 55, No. 10, pp. 30-34, 2003.
9. Johnson, J. L., Tan, L. K., Bollina, R., Suri, P. and German, R. M., “Bi-Metal Injection Molding of Tough/Wear-Resistant Components,” Advances in Powder Metallurgy and Particulate Materials, Part. 8, pp. 262-272, 2003. https://www.cavs.msstate.edu/publications/docs/2003/07/2003-24.pdf (Accessed 19 JAN 2016)
10. Mulser, M., Baumann, A., Ebert, S., Imgrund, P., Langer, I., and Petzoldt, F., “Materials of High Hardness and Wear Resistance Joined to Stainless Steel by 2C-MIM,” Advances in Powder Metallurgy & Particulate Materials, pp. 140-148, 2014.
11. Imgrund, P., Rota, A., and Simchi, A., “Microinjection Moulding of 316L/17-4PH and 316L/Fe Powders for Fabrication of Magnetic-Nonmagnetic Bimetals,” Journal of Materials Processing Technology, Vol. 200, No. 1, pp. 259-264, 2008.
12. Barbosa, A. P. C., Bram, M., Stöver, D., and Buchkremer, H. P., “Realization of a Titanium Spinal Implant with a Gradient in Porosity by 2-Component-Metal Injection Moulding,” Advanced Engineering Materials, Vol. 15, No. 6, pp. 510-521, 2013.
13. Maetzig, M. and Walcher, H., “Assembly Moulding of MIM Materials,” Proc. of European Powder Metallurgy Congress and Exhibition, Vol. 2, pp. 43-48, 2006.
14. Heaney, D. F., Suri, P., and German, R. M., “Defect-Free Sintering of Two Material Powder Injection Molded Components - Part I: Experimental Investigations,” Journal of Materials Science, Vol. 38, No. 24, pp. 4869-4874, 2003.
15. German, R. M., Heaney, D. F., and Johnson, J. L., “Bi-Material Components using Powder Injection Molding: Densification, Shape Complexity, and Performance Attributes,” Advances in Powder Metallurgy and Particulate Materials, Vol. 4, pp. 41-52, 2005.
16. Simchi, A., Rota, A., and Imgrund, P., “An Investigation on the Sintering Behavior of 316L and 17-4PH Stainless Steel Powders for Graded Composites,” Materials Science and Engineering: A, Vol. 424, No. 1, pp. 282-289, 2006.
17. Simchi, A. and Petzoldt, F., “Cosintering of Powder Injection Molding Parts Made from Ultrafine WC-Co and 316L Stainless Steel Powders for Fabrication of Novel Composite Structures,” Metallurgical and Materials Transactions A, Vol. 41, No. 1, pp. 233-241, 2010.
18. Miura, H., Yano, T., and Matsuda, M., “PIM in-Process Joining for More Complicated Shape and Functionality,” Advances in Powder Metallurgy and Particulate Materials, Vol. 10, pp. 295-300, 2002.
19. Baumgartner, R. and Tan, L.-K., “Powder Injection Moulding of Bi-Metal Components,” Proc. of European Powder Metallurgy Congress and Exhibition, Vol. 3, pp. 135-140, 2001.
20. Ruh, A., Dieckmann, A.-M., Heldele, R., Piotter, V., Ruprecht, R., et al., “Production of Two-Material Micro-Assemblies by Two-Component Powder Injection Molding and Sinter-Joining,” Microsystem Technologies, Vol. 14, No. 12, pp. 1805-1811, 2008.

21. Schulze, G., "Die Metallurgie des Schweiβens," Springer, 3rd Ed., p. 198, 2004.

22. German, R. M., "Powder Metallurgy Science," Metal Powder Industries Federation, Princeton, 2nd Ed., p. 251, 1994.

23. Mulser, M., Petzoldt, F., Lipinski, M., and Hepp, E., "Influence of the Injection Parameters on the Interface Formation of Co-injected PIM Parts," Proc. of European Powder Metallurgy Congress and Exhibition, Vol. 2, pp. 159-164, 2011.

24. Li, Y., He, H., Wang, G., and Deng, Z., "Effect of Delay Time on Material Distribution of Metal Co-injection Moulding," Proc. of Powder Metallurgy World Congress and Exhibition, Vol. 4, pp. 511-517, 2010.

25. Olson, D. L., Siewert, T. A., Liu, S., and Edwards, G. R., "ASM Handbook: Welding, Brazing, and Soldering," ASM International, Vol. 6, p. 223, 1993.

26. Kou, S., "Welding Metallurgy," Wiley, 2nd Ed., p. 211, 2002.

27. Bargel, H.-J. and Schulze, G., "Werkstoffkunde," Springer, 6th Ed., p. 182, 230, 1999.

28. Firouzdor, V., Simchi, A., and Kokabi, A. H., "An Investigation of the Densification and Microstructural Evolution of M2/316L Stepwise Graded Composite during Co-Sintering," Journal of Materials Science, Vol. 43, No. 1, pp. 55-63, 2008.

29. Klar, E. and Samal, P. K., "Powder Metallurgy Stainless Steels: Processing, Microstructures, and Properties", ASM International, pp. 127-128, 2007.

30. Metal Powder Industries Federation, "Materials Standards for Metal Injection Molded Parts," http://www.mimaweb.org/std35mim_indiv.pdf (Accessed 29 JAN 2016)